Electronic Supplementary Material (ESI) for Energy & Environmental Science.

A quasi-solid-state rechargeable cell with high energy and superior safety enabled by stable redox chemistry of Li_2S in gel electrolyte

Xiangyu Meng,[a] Yuzhao Liu,[a] Zhiyu Wang,[a,*] Yizhou Zhang,[a] Xingyu Wang,[a] Jieshan Qiu[b,*]

[a] *State Key Lab of Fine Chemicals, Liaoning Key Lab for Energy Materials and Chemical Engineering, PSU-DUT Joint Center for Energy Research, Dalian University of Technology, Dalian 116024, China. Email: zywang@dlut.edu.cn*

[b] *College of Chemical Engineering, Beijing University of Chemical Technology, Beijing 100029, China. Email: jqiu@dlut.edu.cn*

Method

Synthesis of Si-NP@MCNF anode. Free-standing Si-NP@MCNF anodes were made in a similar way of electrospinning *h*-CoN@MCNF fabrics except to replace the $Co(Ac)_2{\cdot}4H_2O$ by commercial Si powder (0.36 g) with an average size of *ca.* 50 nm. The obtained fabrics were aged at 280°C for 2 h in air and subsequently annealed at 800 °C for 2 h in H_2/Ar flow to yield Si-NP@MCNF anode.

Deposition behavior of Li_2S. The deposition behavior of Li_2S on *h*-CoN@MCNF or MCNF was measured by a CHI760A electrochemical workstation in CR2016 coin cells. The *h*-CoN@MCNF or MCNF were used as the working electrode and Li foil was used as the counter/reference electrode. The Li_2S_8 solution (0.25 M) was prepared by mixing the Li_2S and sulfur with a molar ratio of 1 : 7 in 1.0 M LiTFSI in DOL/DME (1:1 by volume) under stirring at 50 ºC for 24 h. A 25 μL Li_2S_8 solution (0.25 M) was applied as catholyte, and the control electrolyte without Li_2S_8 (20 μL) was used as anolyte. The assembled cells were firstly galvanostatically discharged at 0.10 mA to 2.06 V, and subsequently potentiostatically discharged at 2.05 V to fully convert the polysulfides to solid Li_2S on the electrode until the current dropped below 10^{-5} A.

Visualized adsorption test. The Li_2S_6 solution (10 mM) was prepared by mixing sulfur and Li_2S with a molar ratio of 5:1 in DOL/DME (1:1 by volume) via magnetically stirring at 50 °C for 24 h. The *h*-CoN@MCNF or MCNF with a similar surface area of *ca.* 2.0 m^2 were immersed into 4.0 mL of Li_2S_6 solution for 12 h to assure throughout adsorption. Afterward, the supernatant solution was collected for analysis by a UV-vis spectrometer in a wavelength range of 300 - 650 nm.

Symmetrical cell test. The cells were fabricated by directly using *h*-CoN@MCNF or MCNF with a similar area and weight (*ca.* 2 mg cm^{-2}) as both the working and counter electrodes. The

electrolyte is 1.0 M LiTFSI in DOL/DME (1:1 by volume, 50 μL) containing 0.2 M Li_2S_6. Cyclic voltammetry (CV) studies were conducted using a CHI 660A electrochemical workstation between -1.0 to 1.0 V at different scan rates.

Computational method. Density functional theory (DFT) calculations were performed by the Vienna ab initio simulation package (VASP),[1] using the planewave basis set with an energy cutoff of 400 eV, the projector augmented wave (PAW) potentials,[2] and the GGA-PBE exchange-correlation functional.[3] Partial occupancies of the Kohn-Sham orbitals were allowed using the Gaussian smearing method and a width of 0.05 eV. The electronic energy was considered self-consistent when the energy change was smaller than 10^{-5} eV. A geometry optimization was considered convergent when the force change was smaller than 0.02 eV/Å. Grimme's DFT-D3 methodology[4] was used to describe the dispersion interactions. The lattice constant of zincblende-type cubic CoN bulk unit cell is optimized, when using a 9 × 9 × 9 Monkhorst-Pack scheme *k*-point grid for Brillouin zone sampling, to be a = 4.220 Å. Basing on this unit cell, five surface models were constructed as follows.

Co-terminated and N-terminated CoN (100) surface models were built with $p(3\times2)$ periodicity in the x and y directions and 1.5 stoichiometric layers (6 atomic layers) in the z-direction separated by vacuum in the depth of 15 Å to separate the surface slab from its periodic duplicates. Both models contain 36 Co and 36 N atoms. A CoN (110) surface model was built with $p(3\times2)$ periodicity in the x and y directions and 2 stoichiometric layers (4 atomic layers) in the z-direction separated by vacuum in the depth of 15 Å. It contains 48 Co and 48 N atoms. Co-terminated and N-terminated CoN (111) surface models were built with $p(4\times4)$ periodicity in the x and y directions and 3 stoichiometric layers (6 atomic layers) in the z-direction separated by vacuum in the depth of 15 Å. Both models contain 48 Co and 48 N atoms. During structural optimizations, the Γ point in the Brillouin zone was used for *k*-point sampling, and the top two atomic layers were allowed to relax while the bottom four were fixed.

The transition state of the elementary reaction step $Li_2S \rightarrow LiS + Li$ was located by the nudged elastic band (NEB) method.[5] In the NEB method, the path between the reactant(s) and product(s) was discretized into a series of five structural images. The intermediate images were relaxed until the perpendicular forces were smaller than 0.02 eV/Å. The adsorption energy (E_{ads}) of adsorbate A was defined as $E_{ads} = E_{A/surf} - E_{surf} - E_{A(g)}$, where $E_{A/surf}$, E_{surf} and $E_{A(g)}$ are the energy of adsorbate A adsorbed on the surface, the clean surface, and isolated A molecule in a cubic periodic box with a side length of 20 Å and a 1 × 1 × 1 Monkhorst-Pack k-point grid for Brillouin zone sampling, respectively.

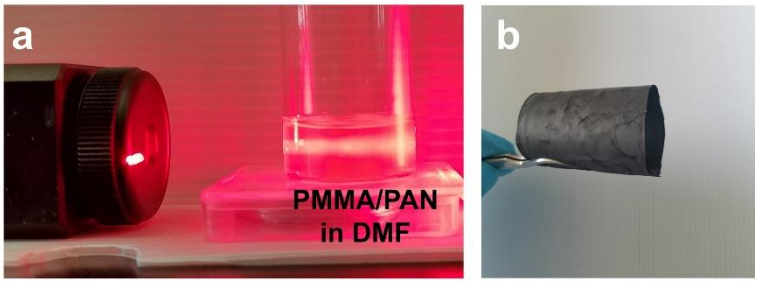

Fig. S1. (a) The Tyndall effect of PMMA/PAN in DMF solution. (b) Optical images of *h*-CoN@MCNF fabric.

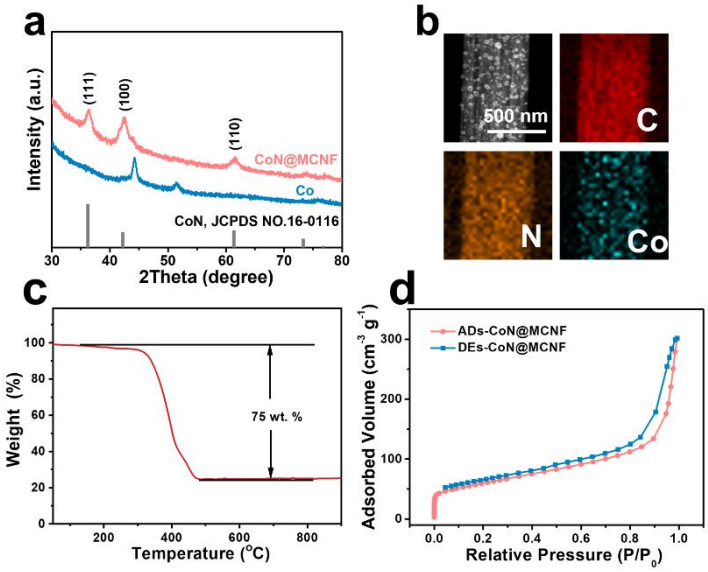

Fig. S2. (a) XRD pattern, (b) element mapping, (c) TGA curve measured in air at a ramp rate of 10 °C min^{-1}, and (d) N_2 adsorption-desorption isotherms of *h*-CoN@MCNF fabrics.

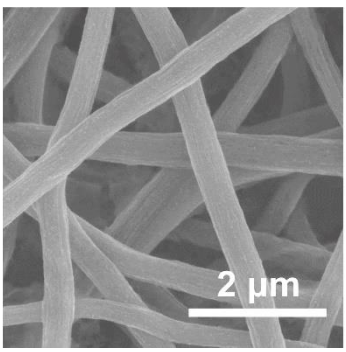

Fig. S3. SEM image of *h*-CoN@MCNF/Li_2S cathode.

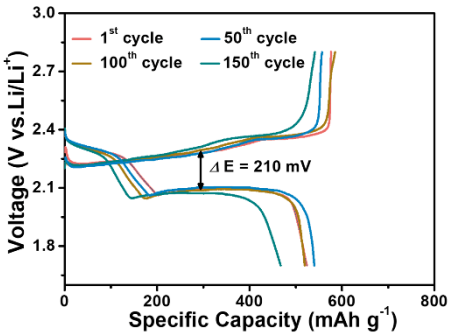

Fig. S4. Discharge-charge voltage profiles of MCNF/Li_2S cathode for different cycles at 0.2 C.

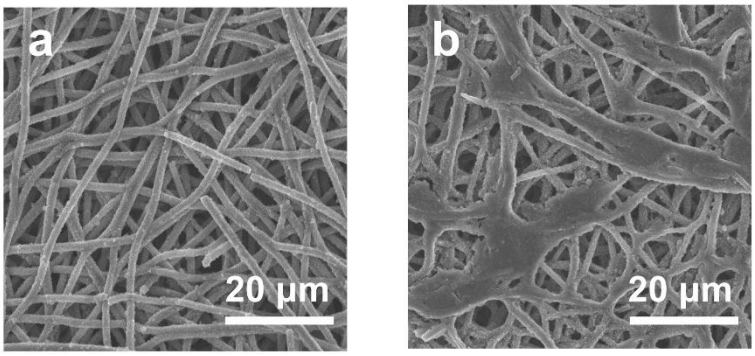

Fig. S5. SEM images of discharged (a) *h*-CoN@MCNF/Li_2S cathode and (b) MCNF/Li_2S cathode.

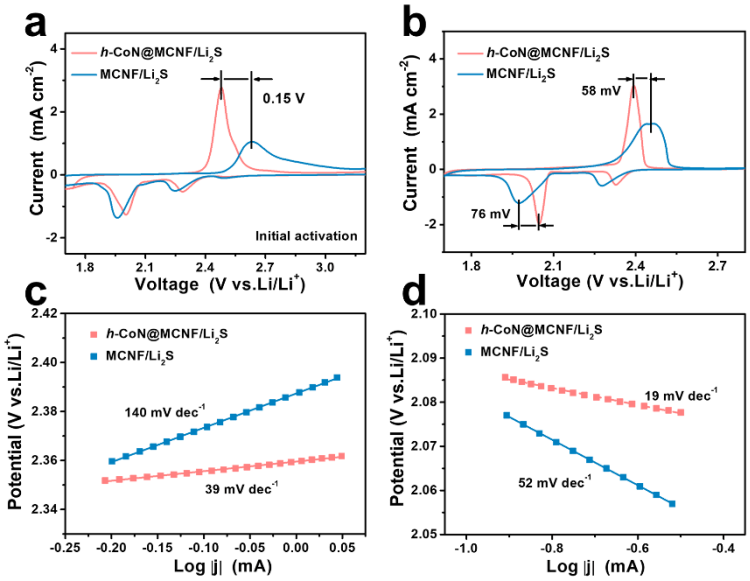

Fig. S6. CVs of *h*-CoN@MCNF/Li_2S and MCNF/Li_2S cathode upon (a) initial cycle between 1.7 and 3.2 V and (b) after initial cycle between 1.7 and 2.8 V at a scan rate of 0.1 mV s^{-1}. Tafel plots derived from (c) oxidation and (d) reduction process of Li_2S.

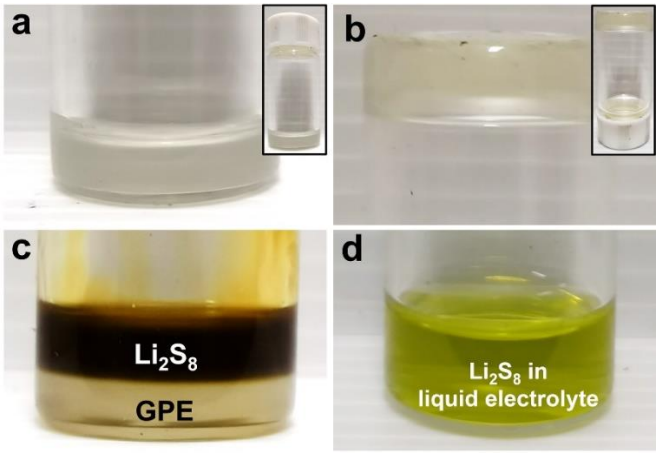

Fig. S7. Optical images of GPE in a glass vessel (a) before and (b) after turning upside down. Permeation capability of Li_2S_8 in (c) GPE and (d) liquid electrolyte.

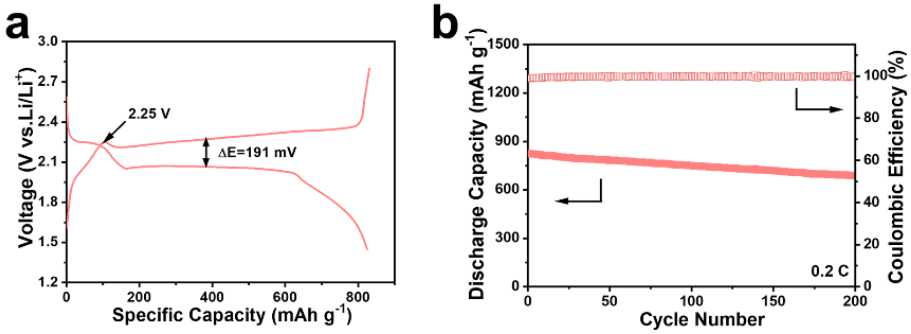

Fig. S8. (a) Typical discharge-charge voltage profiles and (b) cycling stability of *h*-CoN@MCNF/Li_2S cathode in GPE at 0.2 C.

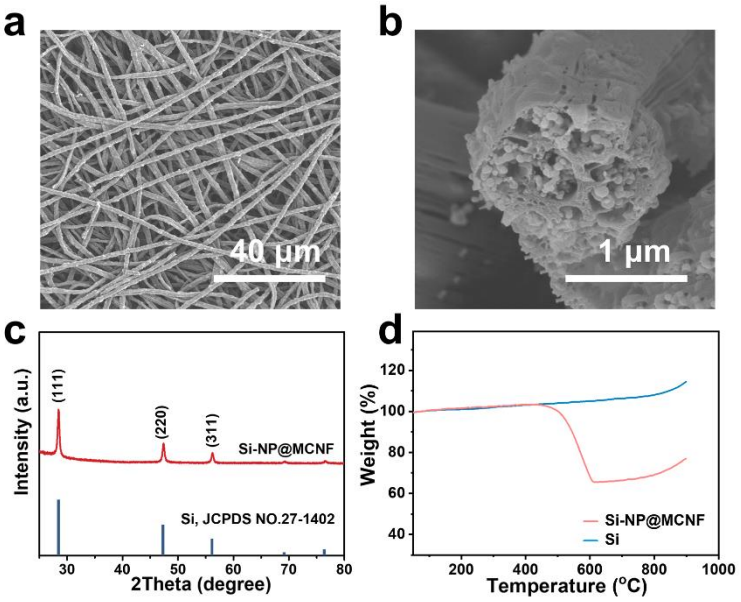

Fig. S9. (a) SEM image, (b) cross-section, (c) XRD pattern and (d) TGA curve of Si-NP@MCNF anode.

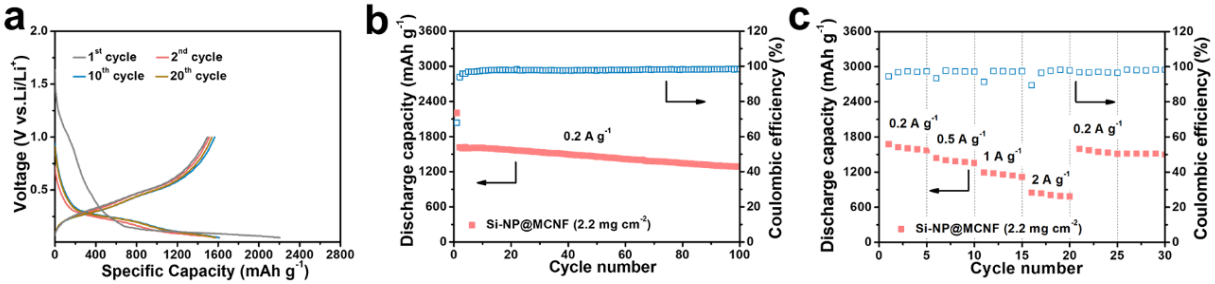

Fig. S10. (a) Discharge-charge curves, (b) cycling stability, and (c) rate performance of Si-NP@MCNF in half cells.

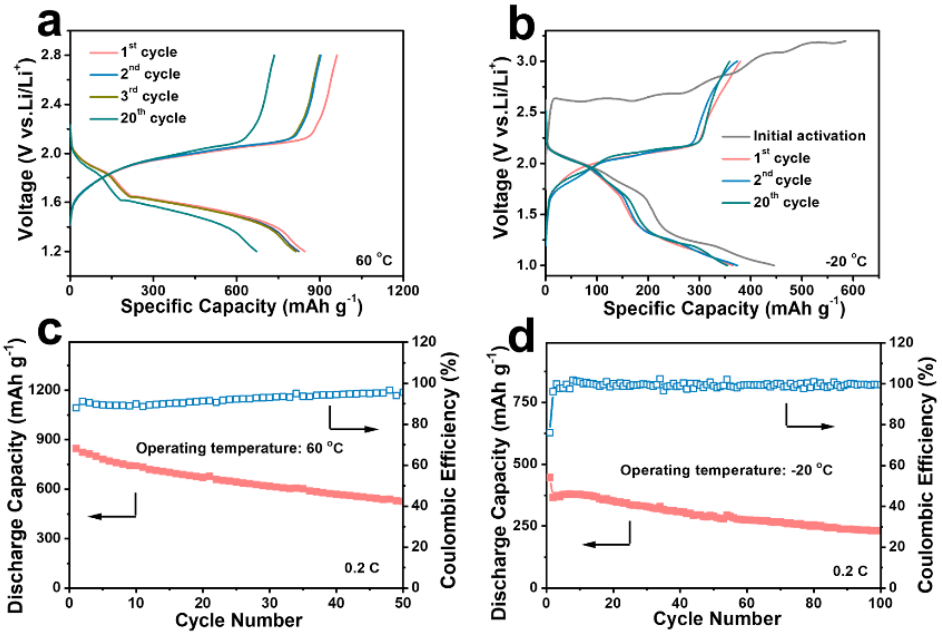

Fig. S11. Discharge-charge voltage profiles and cycling performance of quasi-solid-state Li_2S||Si full cells at (a, c) 60℃ and (b, d) -20 ℃ at 0.2 C.

Fig. S12. OCV of quasi-solid-state Li_2S||Si full cells under (a) initial state, (b) mechanical impact and (c) bending state.

Fig. S13. Optical images of (a) a fresh Li_2S||Si full cell without initial charge, (b) a fully charged Li_2S||Si full cell and (c) a Li-S cell after nail penetration in air. Corresponding infrared thermography is shown in Fig. 5a.

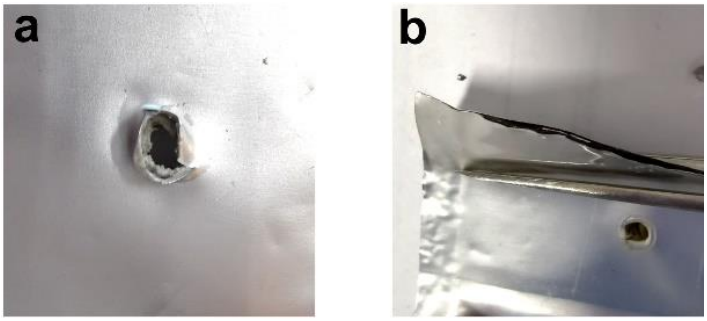

Fig. S14. Optical images of the broken regions on quasi-solid-state Li_2S||Si full cells.

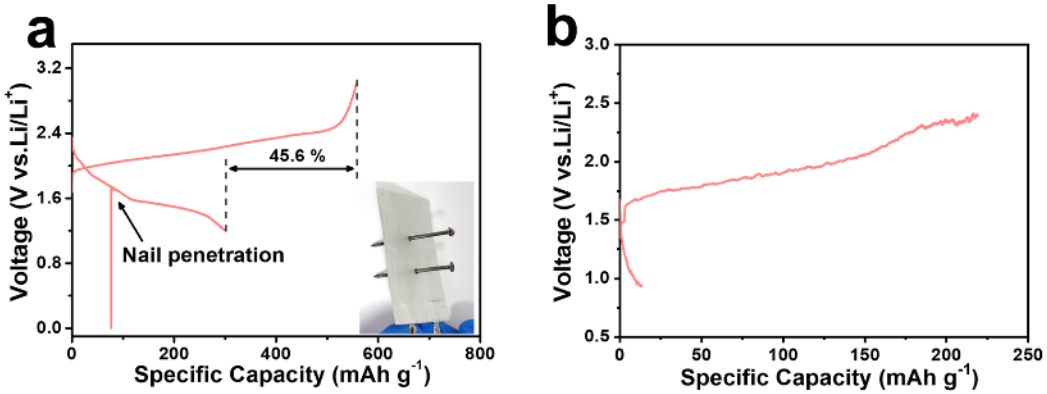

Fig. S15. (a) The charge-discharge curve of quasi-solid-state Li_2S||Si full cells after (a) nail penetration and (b) cutting half in air.

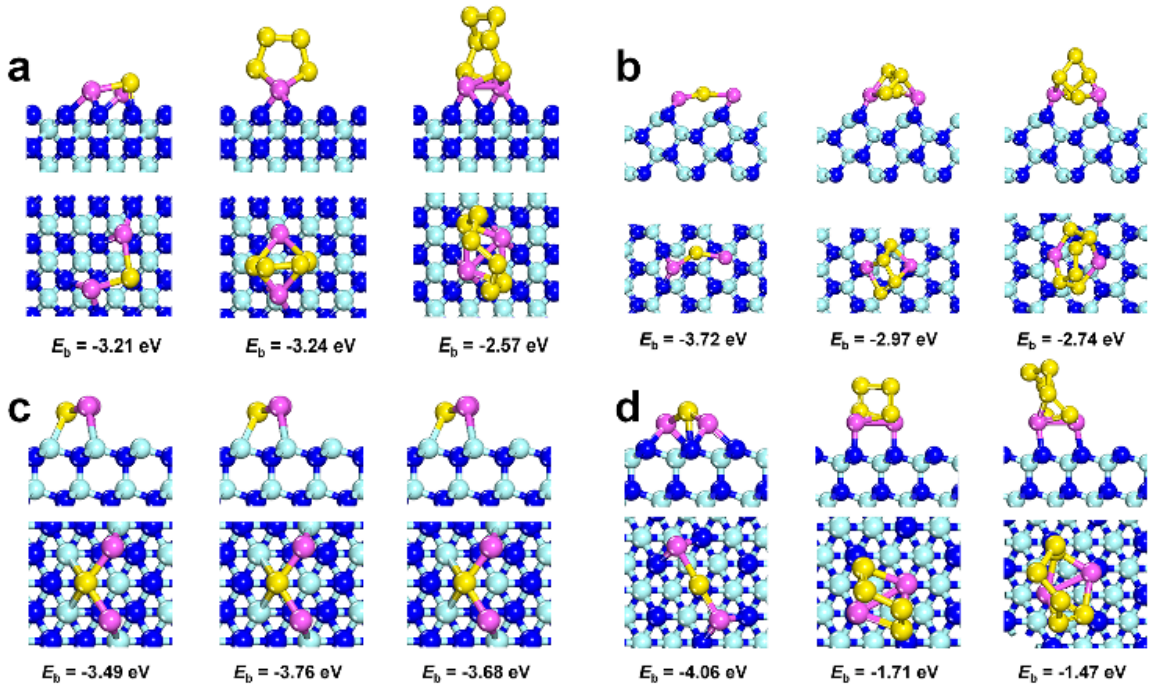

Fig. S16. Atomic structures of Li_2S, Li_2S_4 and Li_2S_6 cluster adsorbed on (a) N-terminated CoN (100) facet; (b) CoN (110) facet; (c) Co-terminated CoN (111) facet, (d) N-terminated CoN (111) facet. The Co, N, Li, and S atoms are shown as spheres in cyan, blue, purple, and yellow, respectively.

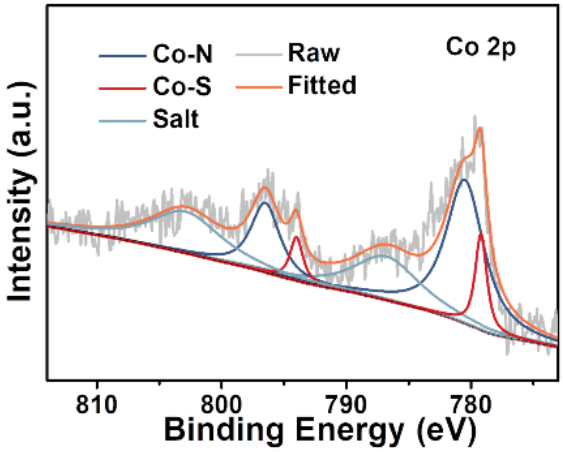

Fig. S17. Co 2p XPS spectrum of *h*-CoN@MCNF/Li_2S cathode after discharge.

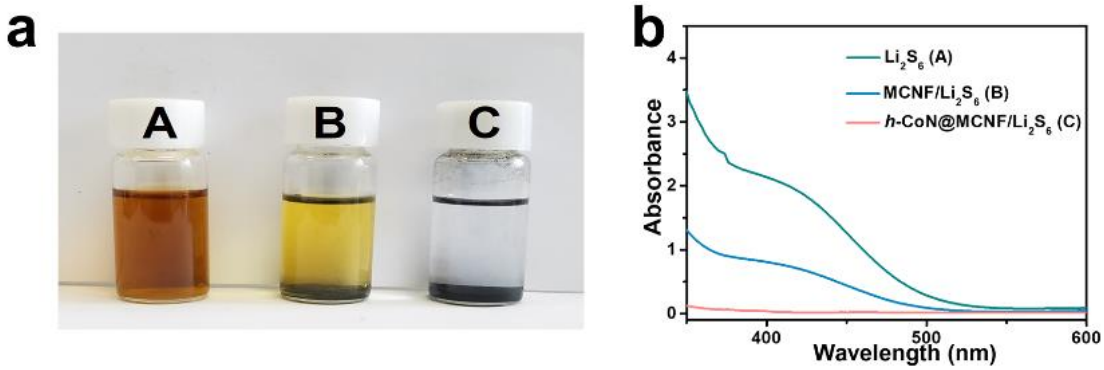

Fig. S18. (a) Optical image of Li_2S_6 solution before and after exposure to *h*-CoN@MCNF or MCNF for 12 h. (b) UV-vis absorption spectra after the adsorption.

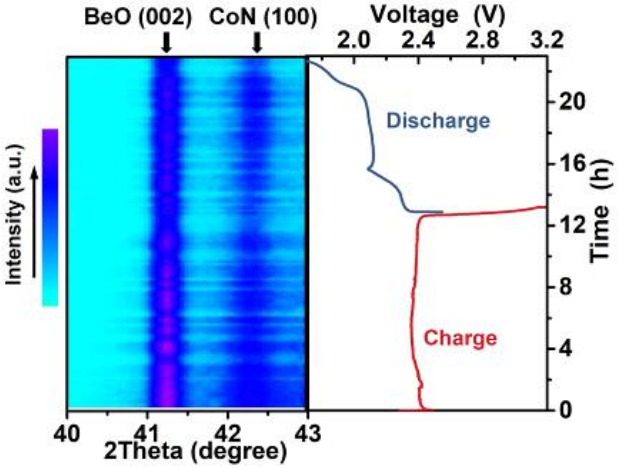

Fig. S19. *In-operando* XRD pattern of CoN in *h*-CoN@MCNF/Li_2S cathode during cycling.

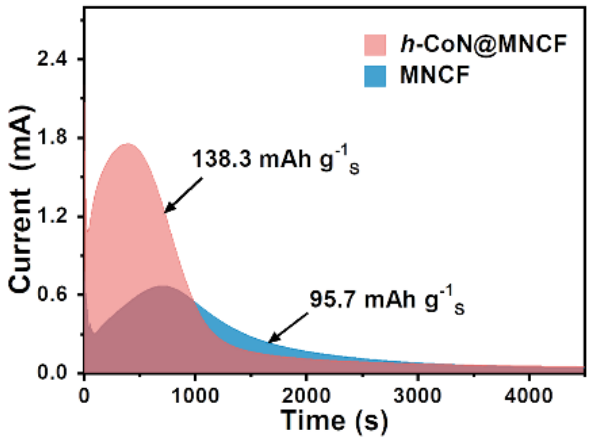

Fig. S20. Potentiostatic discharge profile of Li_2S deposition on *h*-CoN@MCNF and MCNF electrodes at 2.05 V.

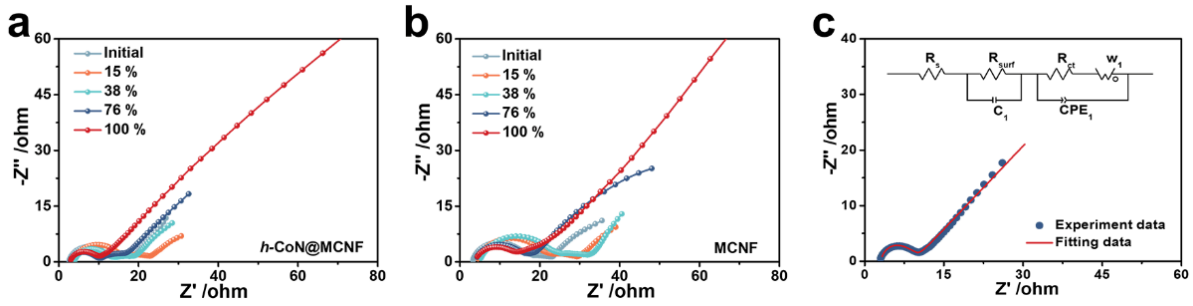

Fig. S21. *In-operando* Nyquist plots of (a) *h*-CoN@MCNF/Li_2S and (b) MCNF/Li_2S cathode at different discharge depth. (c) Fitting result of Nyquist plots of h-CoN@MCNF/Li_2S cathode with 100 % discharge depth, wherein the inset is the equivalent circuit model.

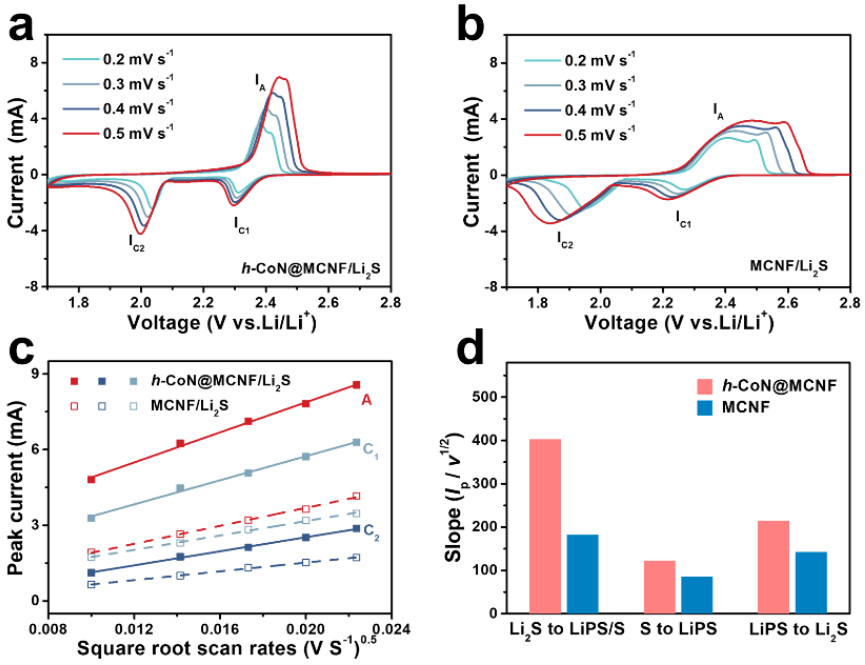

Fig. S22. CVs of (a) *h*-CoN@MCNF/Li_2S and (b) MCNF/Li_2S cathode in half cells at various scan rates from 0.2 to 0.5 mV s^{-1} between 1.7 and 2.8 V. (c) Plot of CV peak current *vs.* the square root of scan rates and (d) derived value of $I_P/v^{1/2}$ for charge and discharge process of *h*-CoN@MCNF/Li_2S and MCNF/Li_2S cathode.

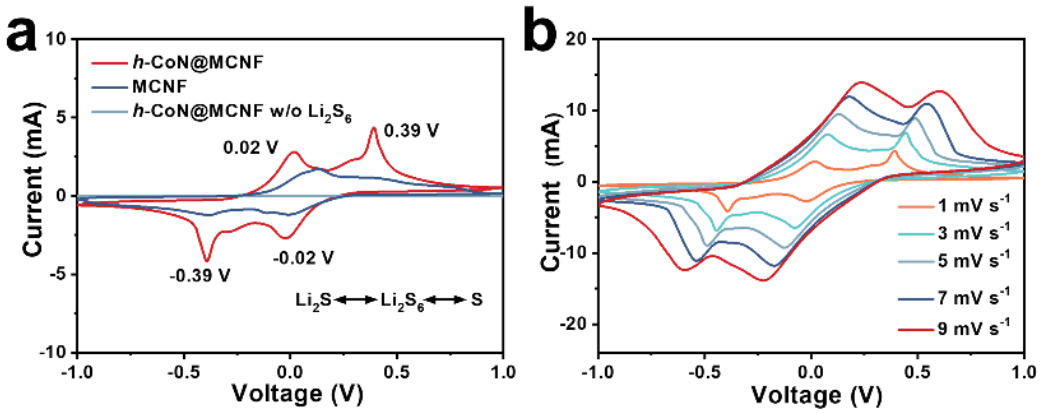

Fig. S23. CVs of the symmetric cells with *h*-CoN@MCNF or MCNF as both the working and counter electrodes, and 1.0 M LiTFSI-DOL/DME with or without 0.2 M Li_2S_6 as the electrolyte at a scan rate of 1.0 mV s^{-1} between -1.0 and 1.0 V. (b) CVs of the symmetric cells using identical *h*-CoN@MCNF electrodes at various scan rates.

Table S1. A comparison of CoN@MCNF/Li_2S cathode with recently reported Li_2S-based cathodes in electrochemical performance.

Electrode	Mass loading (mg cm^{-2})	Li_2S content (wt.%)	Specific Capacity based on Li_2S (mA h g^{-1})	Cycle life	Capacity retention (%)	Activation voltage (V)	Reference
Li_2S@$LiTiO_2$	1.2	57.6	732@0.5C	400	88	2.76	6
Li_2S@TiS_2	1.0	51.0	666@0.5C	400	77	3.00	7
Li_2S@ZnS	2.0	62.6	832@0.2 C	100	77	2.87	8
Li_2S@graphene	1.2	42.0	750@0.2C	100	37	2.85	9
Li_2S@graphene	10.0	79.6	533@0.1C	200	54	2.74	10
Li_2S@N,P-C	2.0	62.0	1000@0.1C	100	70	2.65	11
Li_2S@C	1.5	58.7	972@0.2C	100	79	2.80	12
Li_2S@TiN	2.5	--	789@0.2C	100	84	2.87	13
Li_2S@Mo	2.9	25.9	618@0.5 C	500	62	2.57	14
_h_-CoN @MCNF/Li_2S	**2.5**	**65.0**	**820@0.2 C**	**200**	**97.6**	**2.43**	**This work**

Table S2. A comparison of Li_2S-based full cells developed in this work and literature in electrochemical performance.

Battery system	Current rate (C)	Cycle life	Li_2S loading (mg cm^{-2})	Specific energy based on active mass (W h Kg^{-1})	Specific energy based on electrode weight (W h Kg^{-1})	Reference
Li_2S-PAN||Si	0.1	50	1.8	710	165	15
Li_2S/CMK-3||Si NW	0.12	20	1.4	630	124	16
Li_2S||SnO_2	0.5	200	2.4	442	185	17
Li_2S@NCNF||Fe_3O_4/CNs	0.2	50	1.6	675	247	18
Li_2S/graphene||Si-LP	0.08	40	1.3	723	187	19
Li_2S@MXene/G|| Fe_3O_4/CNs	0.2	50	1.8	536	217	20
Li_2S-ZnS@NC|| Si-NP@HCF	0.2	200	2.0	673	256	8
Li_2S-MCMB||Si-O-C	0.2	50	1.0	390	118	21
_h_-CoN@MCNF/Li_2S|| Si-NP@MCNF	**0.2**	**100**	**1.0-2.5**	**802**	**506**	**This work**

* The weight of the electrode includes the mass of active materials, binder, conductive carbon, and metal current collectors.
** The mass of metal current collectors (Cu or Al) is defined as 5 mg cm^{-2}.

Supplementary References

1. Kresse, G.; Furthmüller, J. *Phys. Rev. B* ***54***, 11169 (1996).
2. Kresse, G.; Joubert, D. *Phys. Rev. B* ***59***, 1758 (1999).
3. Perdew, J. P.; Burke, K.; Ernzerhof, M. *Phys. Rev. Lett.* **77**, 3865 (1999).
4. Grimme, S.; Antony, J.; Ehrlich, S.; Krieg, H. *J. Chem. Phys.* **132**, 154104 (2010).
5. Henkelman, G.; Uberuaga, B. P.; Jónsson, H. *J. Chem. Phys.* **113**, 9901(2000).
6. Wu, F. X. *et al.*; *Energy Environ. Sci.* **11**, 807-817 (2018).
7. Seh, Z. W. *et al.*; *Nat. Commun.* **5**, 5017 (2014).
8. Yu, M. L. *et al.*; *Adv. Funct. Mater.* **29**, 1905986 (2019).
9. Liang, X. *et al.*; *Chem. Commun.* **55**, 10088-10091 (2019).
10. Tan, G. q. *et al.*; *Nat. Energy* **2**, 17090 (2017).
11. Zhang, J. *et al.*; *Adv. Energy Mater.* **7**, 1602876 (2017).
12. Nan, C. *et al.*; *J. Am. Chem. Soc.* **136**, 4659-4663 (2014).
13. Hao, Z. *et al.*; *Small* **15**, e1902377 (2019).
14. Xing, Z. Y. *et al.*; *Adv. Mater.* **32**, 2002403 (2020).
15. Shen, Y. F. *et al.*; *ACS Energy Lett.* **4**, 1717-1724 (2019).
16. Yang, Y. *et al.*; *Nano Lett.* **10**, 1486-1491 (2010).
17. Liu, M. *et al.*; *Nano Energy* **40**, 240-247 (2017).
18. Yu, M. L. *et al.*; *Adv. Energy Mater.* **7**, 1700018 (2017).
19. Li, Z. *et al.*; *Electrochemistry* **84**, 887-890 (2016).
20. Wang, Z. Y. *et al.*; *J. Energy Chem.* **37**, 183-191 (2019).
21. Agostini, M. *et al.*; *ACS Appl. Mater. Interfaces* **6**, 10924-10928 (2014).